Development of Soft X-ray Tracer Diagnostics for Hohlraum Experiments

J.J. MacFarlane, D.H. Cohen, P. Wang,
R.R. Peterson, G.A. Moses, C.A. Back,
O.L. Landen, R.J. Leeper, R.E. Olson, T. Nash

April 1998

UWFDM-1069

FUSION TECHNOLOGY INSTITUTE

UNIVERSITY OF WISCONSIN

MADISON WISCONSIN

Development of Soft X-ray Tracer Diagnostics for Hohlraum Experiments

J. J. MacFarlane, D. H. Cohen, P. Wang, R. R. Peterson, and G. A. Moses

Fusion Technology Institute
University of Wisconsin–Madison
1500 Engineering Dr.
Madison, Wisconsin 53706

In collaboration with:

C. A. Back, O. L. Landen (LLNL)
and
R. J. Leeper, R. E. Olson, T. Nash (SNL)

April 1998

UWFDM-1069

Contents

1. Introduction

The purpose of this report is to summarize work performed by the University of Wisconsin during fiscal year 1996 under the NLUF contract DE-FG03-96SF21015. This contract involved the development of soft x-ray spectral diagnostics from tracer layers in hohlraum witness plates. This effort was originally intended to be focused on OMEGA experiments, but the experiments were changed to NOVA because initial indirect drive shots had not yet been performed on the OMEGA upgrade. Data were collected in a series of experiments between January 1997 and October 1997. Experiments were delayed somewhat due to bringing up the Hettrick spectrometer on the NOVA target chamber. The tasks related to the planning, carrying out, and modeling of the experiments are outlined in Table 1.1 and detailed in the remainder of this report.

Table 1.1. Tasks for Fiscal Year 1996

1. Model hydrodynamics, atomic properties, and emergent spectra in order to plan experiments and target fabrication.
2. Oversee target fabrication by Luxel.
3. Organize and perform experiments at Livermore, in collaboration with Dr. Christina Back.
4. Perform end-to-end modeling of experiments and make quantitative comparisons to the data.
5. Publish results in reports, conference proceedings, and papers.

The tracer emission spectroscopy is a useful diagnostic of time-dependent hohlraum radiation conditions. Our initial calculations showed that in addition to providing information on the intensity of the radiation field, the spectra could be used to measure the timing of the radiation wave and the frequency-dependent albedo of a material sample. The experiments we describe and model here, because they are the first to explore this technique, were relatively straightforward in the sense that they employed aluminum witness plates and,

for the most part, square laser pulses. The properties of aluminum are well known, so these experiments serve to test and benchmark the diagnostic techniques.

The buried tracer layers (sub-micron layers of KCl or MgF_2) become hot ($T_e > 100$ eV) very rapidly when the radiation wave arrives. The time-dependent self-emission from these layers is observed through a diagnostic hole opposite the witness plate and recorded by a streak camera. The experimental conditions are further constrained by mid-plane DANTE measurements of wall reemission and SOP measurements of the shock breakout on the back of the Al witness plate.

These soft x-ray spectral diagnostics in the hohlraum environment are important for the promise they hold for improving our understanding of both hohlraum and capsule physics, and hence for ultimately achieving ignition in an indirect-drive ICF setting. By providing more detailed and quantitative measurements of the radiation conditions inside hohlraums than the broad-band DANTE instrument allows, they will enable researchers to explore the details of hohlraum radiation fields, such as their time-variability and deviations from a pure blackbody spectrum. Additionally, the albedo and radiation wave velocity measurements made possible by tracer spectroscopy will be useful for testing the properties of materials that can be used in the hohlraum environment, whether as ablators or as part of the hohlraums themselves. Clearly, this type of information will be very important for efficiently coupling the hohlraum radiation field to the capsule and optimizing the performances of both hohlraum and capsule materials.

The techniques explored in our experiments and modeling have several unique aspects that may prove advantageous when used in conjunction with other types of diagnostics:

1. Sub-kilovolt spectroscopy of the hohlraum interior – this is the wavelength regime where most of the drive energy is concentrated.

2. Low-Z tracers buried in aluminum – gives a high contrast background for the emission signal.

3. Tracers are buried under a tamper (1 μm to 5 μm) – mitigates expansion and contamination from gold blow-off.

4. Makes use of combined spectroscopy and absolutely calibrated XRD data.

5. Multiple tracer layers – allows for the measurement of the speed of x-ray wave propagation inside a sample.

These experiments and related modeling efforts are the first step in a larger exploration of tracer spectroscopy in indirect-drive ICF settings. We will soon be performing tracer *absorption* spectroscopy experiments at OMEGA in order to characterize plastic ablator properties. Tracer absorption diagnostics are complementary to the emission spectroscopy, and both rely on a time-dependent, localized measurement of properties of the *interior* of a sample. Both also require the use of detailed atomic, hydrodynamic, and non-LTE collisional-radiative modeling.

The goals of the experiments discussed in this report are:

1. To spectrally observe line emission from buried tracers in hohlraums;

2. To determine what tracers and tracer properties are optimal;

3. To provide constraints on the hohlraum radiation field;

4. To determine over what range of temperatures these diagnostics will be useful.

In the remainder of this report we will discuss the experiments that were carried out (§ 2), show some of the data (§ 3), detail our modeling of the data (§ 4), and discuss our conclusions and future directions for the development of spectral diagnostics from thin tracer layers in hohlraums.

2. Experiments

All of the experiments described in this section took place at the NOVA laser at Lawrence Livermore National Laboratory during calendar year 1997. They all involved stepped aluminum witness plates mounted on the sides of scale-1.5 gold hohlraums. A sketch of the hohlraum experimental set-up and witness plate is shown in Figure 2.1. Note that the primary diagnostic is the Hettrick soft x-ray spectrometer, fielded by Dr. C. Back with the assistance of Dr. T. Nash. These experiments represent the first attempts to use this spectrometer in the hohlraum environment. Note also that the witness plates were coated by Luxel, and that the tracer and aluminum layer thicknesses and densities are known to within 10%.

Three preliminary shots were performed in January 1997. One of these included a modified diagnostic configuration in which the DANTE diagnostic looked at the aluminum witness plate. In general, however, the spectroscopy from these shots was limited by exposure problems. With the knowledge of exposure levels and photocathode options gained in the January experiments, we went back into the lab in October 1997 and performed nine shots over a two day period. The tracer spacings and thicknesses varied from shot to shot, as did the spectrometer's slit-width and the streak camera's sweep speed. In some shots, the KCl and MgF_2 tracer layers were adjacent, and in others the KCl tracer was up to 10 μm farther from the hohlraum-facing surface of the witness plate than was the MgF_2 layer.

For all shots except the final one, we used a 1 ns square laser pulse. In general, a peak hohlraum radiation temperature of 200 eV was achieved, although on several shots only nine beams fired and the temperature was correspondingly lower. On the last shot, we used a shaped pulse (pulse shape 26) with a long, low-temperature foot followed by a high-temperature peak.

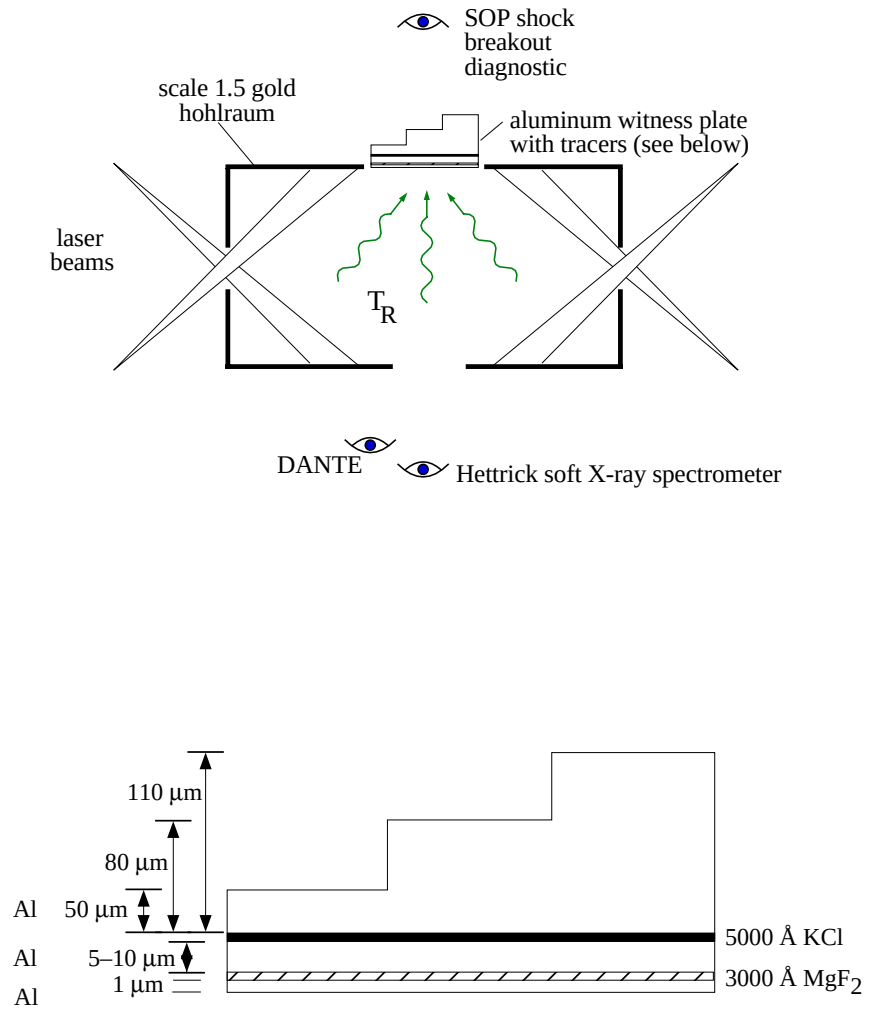

Figure 2.1. The top portion of this figure shows a cut-away of the hohlraum experimental set-up. DANTE and spectrometer diagnostics view the hohlraum wall and witness plate, respectively, through a diagnostic hole opposite the witness plate. The SOP makes a shock breakout measurement on the back, stepped side of the witness plate. All three of these diagnostics are time-resolved. A cross section of a typical witness plate is shown in the bottom portion of the figure. Each thin tracer layer is covered by an additional layer of aluminum, leading to a situation in which the tracers are buried under at least a micron of aluminum on the hohlraum-facing side of the witness plate. The thicknesses of the tracers and aluminum layers vary from shot to shot. Neither figure is drawn to scale.

3. Data

Shot number 27101504 (1504), the first shot of 15 October 1997, was typical of the data collected during our October 1997 campaign. Both tracer layers were 3000 Å thick in this target, and they were adjacent with the MgF_2 in front and the KCl in back. The Al tamper was 1 μm thick, and the laser pulse was a 1 ns square pulse. A series of line-outs from the time-resolved Hettrick soft x-ray spectrometer is shown in Figure 3.1.

This data set is typical of our October shots in several respects. The sensitivity is such that time-integrations must be done over at least 200 ps in order to get a strong signal in more than a few lines. We see significant spectral evolution on the order of several 100 ps. The instrumental resolution peaks at about $\lambda/\Delta\lambda = 500$ near 25 Å, and falls to roughly $\lambda/\Delta\lambda = 200$ by 15 Å. This was determined from a follow-up calibration disk shot viewed through a mask with machined slits.

In this, and all, shots, the strongest features are due to Lyman-series and He-like lines of fluorine. In a few early shots the grating was adjusted to pick up the corresponding Mg lines near 8 Å, but these features were weak. All shots also show evidence of oxygen. Due to its appearance at early times and its transition to absorption at late times, we suspect that the source of the oxygen is a thin layer of oxidized aluminum on the front of the witness plates. Luxel confirmed the presence of a thin (few hundred Å) layer of aluminum oxide on the coated witness plates. In all of the shots, the deep O I bound-free absorption feature is seen at 23 Å. Because of its ubiquity, stability, and lack of ionization it is assumed to be due to oxygen in the spectrometer; probably on the CsI photocathode.

The K and Cl features are quite weak in this shot, and even weaker in others. It should be noted that the F (and O) features are due to K-shell transitions, while L-shell features of K and Cl are seen in this wavelength regime. In order to see if the weakness of the emission lines was due to K and Cl being ionized beyond Li-like, we performed one shot

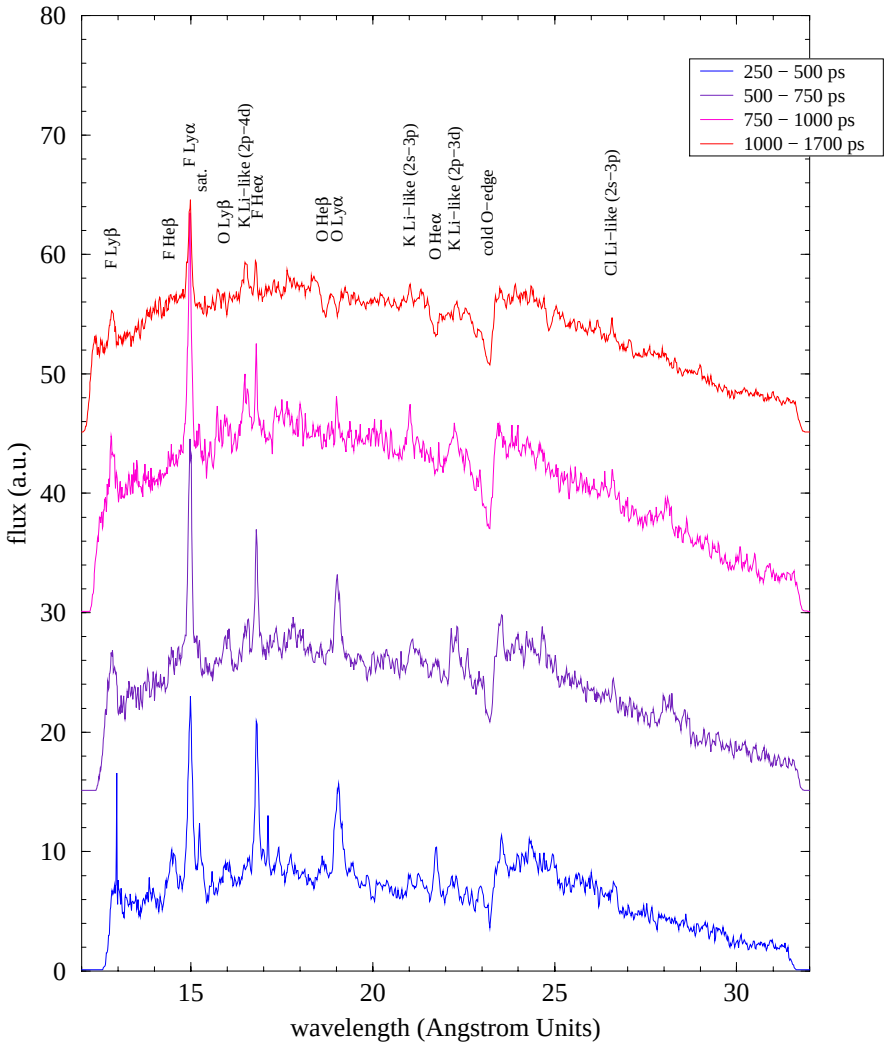

Figure 3.1. Four line-outs from shot 1504 are plotted, with each being offset for clarity. The early line-outs span 250 ps, and the last one, 700 ps. Major features are labeled at the top, although there are several weaker, unlabeled features too, mostly due to K and Cl. These data have not been corrected for the instrumental throughput or the detector sensitivity, so the continuum shape is not physical.

(number 1517) with pulse shape 26, which has a low-temperature foot. The target had the same specifications as the one used in shot 1504. As can be seen in Figure 3.2, the K and Cl features in this data set are somewhat stronger than those seen in the data from shot 1504. This is tentatively taken as evidence that weakness of the features from these species in the square-pulse shots was due to over-ionization.

We also collected shock breakout data from the streaked optical pyrometer (SOP). These data consist of three times, corresponding to the breakout on each of the three steps (with thicknesses of 50 μm, 80 μm, and 110 μm). We show the SOP data in the next section along with models of the shock breakout, based on a drive temperature profile derived from the DANTE data. DANTE gives absolutely calibrated (to within 25%) x-ray fluxes reemitted from the hohlraum wall in ten energy channels. These fluxes are generally used to derive an equivalent blackbody temperature, although the hohlraum radiation field has some deviations from a Planck spectrum. In Figure 3.3 we show the measured effective temperatures, which are recorded with 100 ps time resolution. Also in this figure we show the albedo-corrected temperature profile.

The albedo correction is an attempt to recover the total, angle-integrated flux incident upon the witness plate from a measurement of the reemitted flux. The gold wall reemission measured by DANTE is only one source of hohlraum radiation. The laser hot spots and holes (laser entrance and diagnostic) must also be accounted for when totaling the sources and sinks of radiation. We derived the albedo correction by performing a one-dimensional radiation-hydrodynamics calculation of energy deposition into a gold slab. We adjusted the input radiation temperature profile and monitored the reemitted radiation temperature profile until it matched the observed DANTE profile. The input profile was then taken to be the total hohlraum radiation field profile, and was used as a basis for the modeling discussed in the next section.

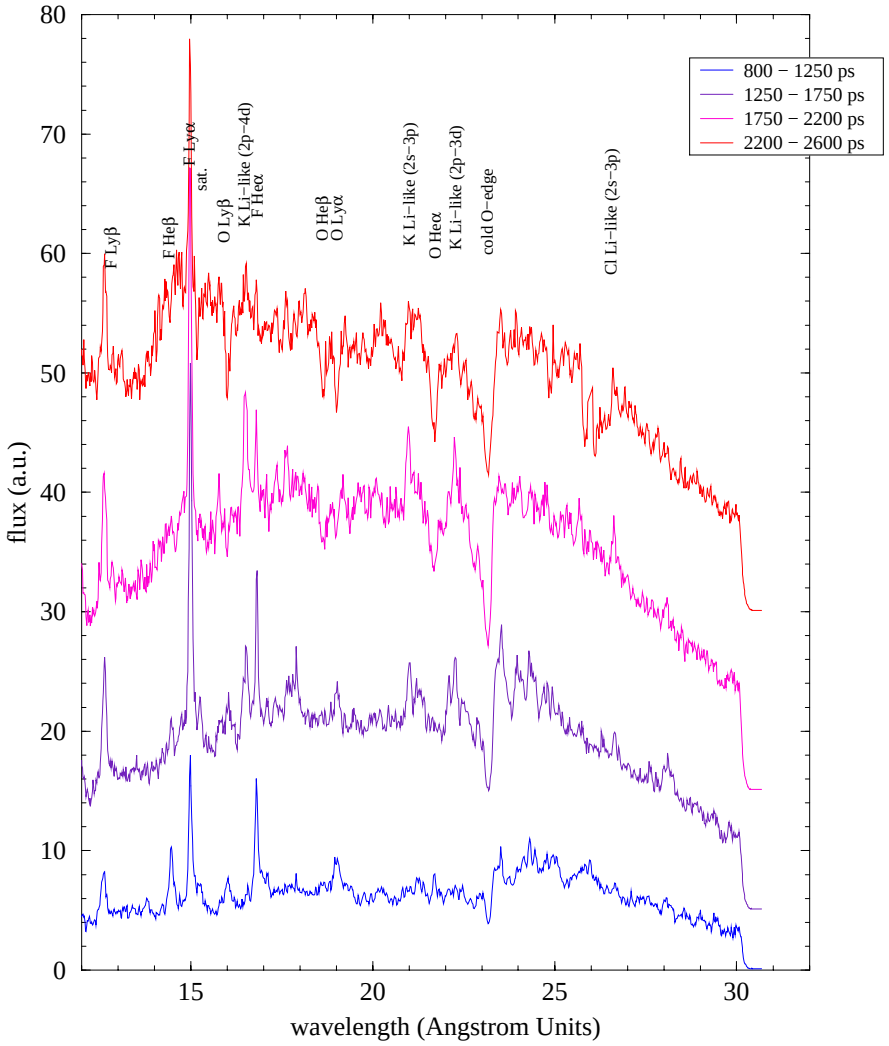

Figure 3.2. Four line-outs from shot 1517 are plotted, with each being offset for clarity. The line-outs span longer time intervals than for the previous figure, as the laser pulse length is longer (2.6 ns). The labels are the same as for the data from shot 1504.

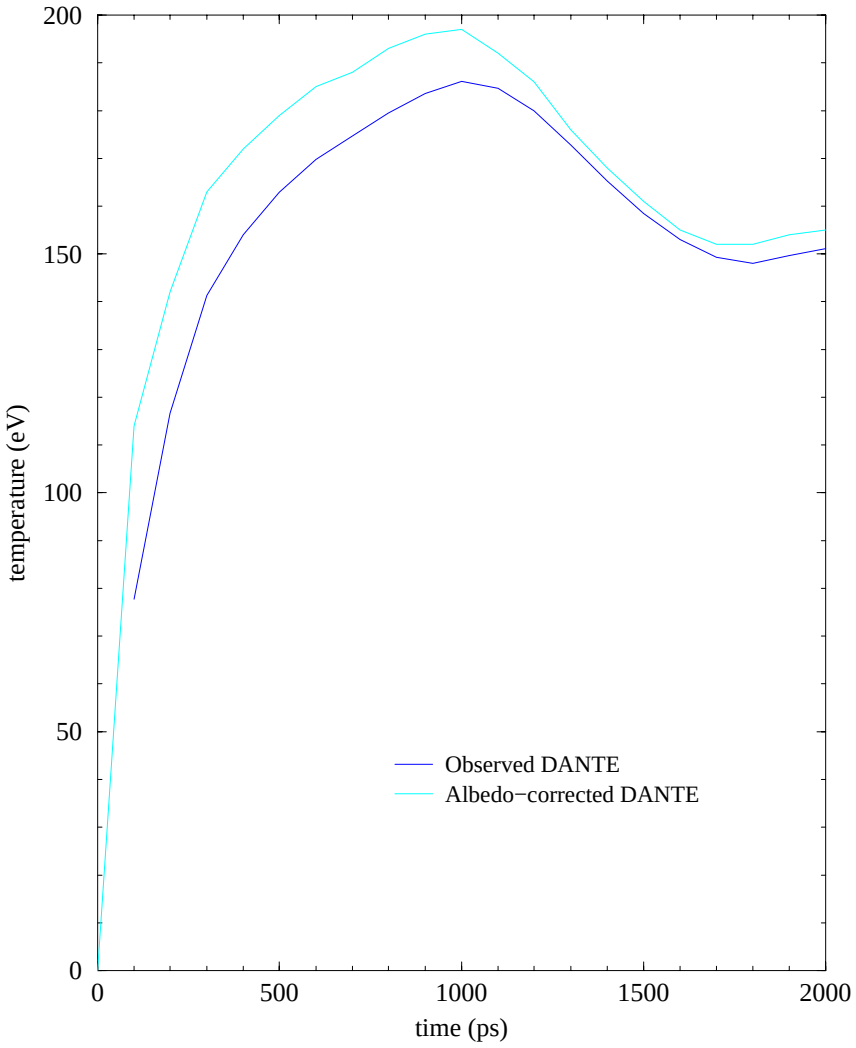

Figure 3.3. The DANTE temperature profile measured for shot 1504 is shown along with the albedo-corrected profile.

4. Models

We have made some preliminary spectral models of selected shots in order to understand basic trends in the data and to evaluate the different diagnostics. A paper, to be submitted to *Phys. Rev. Lett.*, is in preparation. Another paper, focusing more on the spectral modeling, is also in preparation.

Modeling the data from the NOVA experiments discussed in the previous section took place in three stages: (1) constructing atomic models; (2) performing radiation-hydrodynamics calculations of the witness plate exposed to a time-varying hohlraum radiation field; and (3) post-processing the hydrodynamics output using a collisional-radiative equilibrium (CRE) code. Hydrodynamics calculations were also performed in order to make the albedo correction to the DANTE data, as described in § 3.

We calculated atomic models for O, F, Mg, Al, Cl, and K in order to completely model the witness plates with tracers (and the oxidized Al layer). These models include equations of state (EOS) and multi-group (500 frequency groups) opacities for the hydrodynamics calculations. These opacity calculations employed a unresolved transition array (UTA) model for high-Z species and a detailed configuration accounting (DCA) model for low-Z species. A LTE plasma model was used for the EOS in the low-density regime, and a muffin-tin model in the high-density regime. Comparisons between our Al EOS model and the SESAME EOS model of Al showed no discernible difference in numerical hydrodynamics output. Detailed atomic structure models were also made for each element. These employed the Hartree-Fock method in a DCA scheme, and include all relevant collisional and radiative rates. Models for important ionization stages typically included 50 levels.

Using the albedo-corrected DANTE time-dependent radiation temperature profiles (*e.g.* the upper line in Figure 3.3) as a boundary condition, we performed multi-group radiation-hydrodynamics simulations of the witness plates using our one-dimensional

Lagrangian code, BUCKY-1. These calculations assumed LTE (for the EOS/opacity models) and typically used 40 radiation groups. They were used to predict time-dependent density and temperature distributions, as well as multi-group emergent fluxes.

Detailed spectra were calculated using our one-dimensional CRE code, NLTERT. Temperature, density, and spatial distributions were taken from the BUCKY-1 calculations and used as input for the (post-process) CRE calculations. The NLTERT code assumes a time-dependent radiation field (generally Planckian) at the hohlraum-facing boundary of the witness plate. Radiation transfer and statistical equilibrium equations are solved self-consistently in order to synthesize spectra for comparison with the Hettrick spectrometer data.

As a consistency check, we compared the results of the hydrodynamics calculations to the SOP data of the shock breakout on the back of the stepped witness plates. We show a typical result in Figure 4.1. Using the nominal albedo-corrected DANTE radiation temperature profiles for shot 1504 we find shock velocities which are slightly low (of order 12%). By increasing the radiation temperature by 6% (equivalent to the nominal 1 σ DANTE uncertainty), we get very good agreement with the SOP shock breakout data (which itself has 50 ps uncertainties). This level of agreement is not atypical for NOVA witness plate experiments for which there are both DANTE and SOP measurements.

Using the albedo-corrected DANTE data as an input, we have synthesized spectra that correspond to the line-outs for shot 1504 shown in Figure 3.1. This synthesized time series is shown in Figure 4.2. There is good qualitative agreement between this model and the data shown in the previous section: The fluorine Lyman series and helium series dominate the spectra, along with the oxygen features. Note, however, that the O features remain in emission beyond 1.0 ns, unlike in the data. It is not until about 2 ns that our models show the O going into absorption. This may be due to the one-dimensional nature of our calculation. Note also that we do not see the Al L-shell edge near 30 Å in the data, although

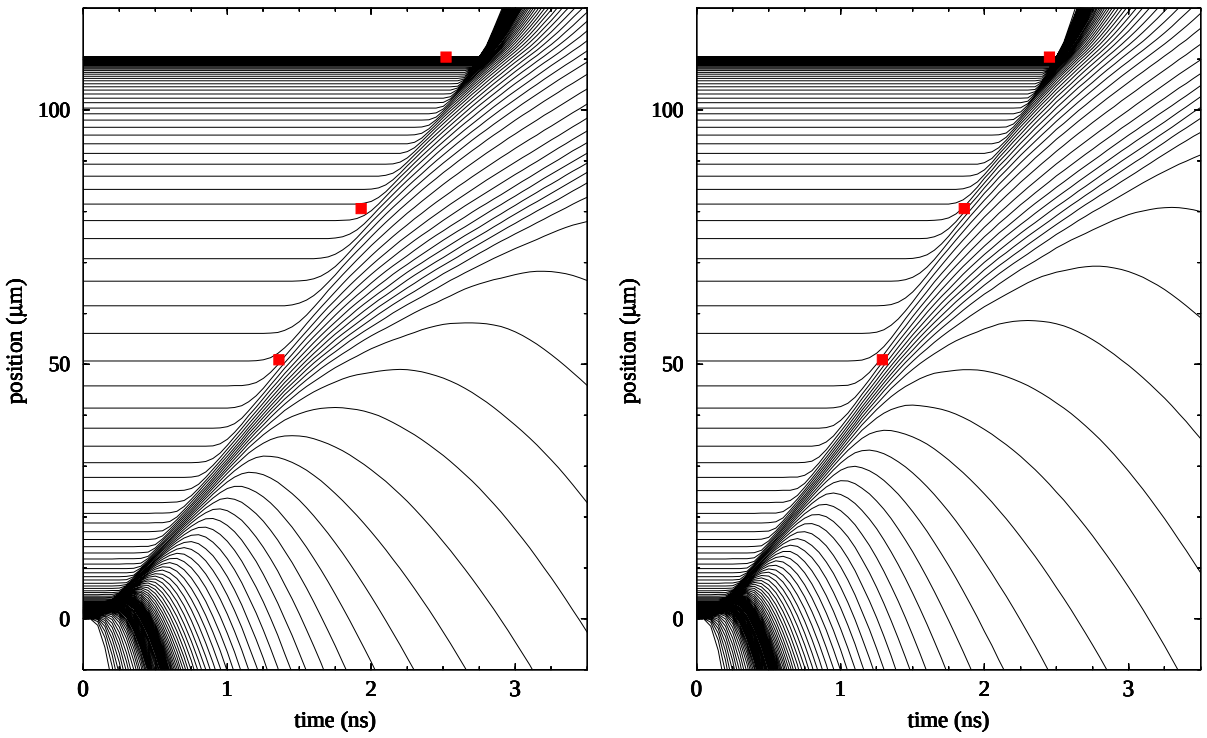

Figure 4.1. Shock breakout simulations for shot 1504. Plotted are positions of Lagrangian computational cells as a function of time, in black, and SOP data points, in red. The diagonal locus caused by abrupt changes in the cell positions represents the position of the shock front as a function of time. Its slope corresponds to the shock velocity. The panel on the left uses the nominal albedo-corrected DANTE data as input for the BUCKY-1 calculation. This calculation gives a shock velocity that is somewhat less than the SOP data indicates. The panel on the right uses the albedo-corrected DANTE temperatures increased by 6% at all times (1 σ uncertainty). Here the agreement with the SOP data is excellent.

it is apparent in the model. This may be due to the poor sensitivity of the detector at this relatively long wavelength.

In order to illustrate details and trends in the evolution of these spectra, we show an expanded view of a portion of the wavelength range in Figure 4.3. Like the data, this model shows that the fluorine lines are strong earlier than the potassium lines (despite the two tracer layers being adjacent for this shot). Furthermore, it reproduces the behavior of the F He-like lines, which weaken with time, much more so than do the F Lyman series lines. Additionally, we see the F Ly α satellite weakly in emission at early times, but going into absorption at later times in the calculation. The data are noisy, but are not inconsistent with this trend. The transition from emission to absorption of the satellite feature is due to the decrease in the electron density with time in the tracer layer, which causes the upper level of the satellite transition to be much less efficiently populated by dielectronic recombination.

The behavior of the satellite feature can be understood only in terms of a non-LTE model. In Figure 4.4 we compare LTE and CRE models at three different times. The primary difference, aside from the F Ly α satellites, is the decreased strength of He-like F features in the CRE models. This is due to the different charge state distributions in the two cases. The features near 9 Å are Mg Ly_α and He_α. Note the difference in the satellite lines between the LTE and CRE cases.

One application of the tracer spectroscopy is an albedo diagnostic. The strength of a pure scattering resonance line is controlled by the radiation field, and in the case of a completely optically thick line, will approach the level of the incident radiation field at the line's frequency. Meanwhile, the observed continuum level reflects the reemission of the aluminum. Thus, taken together, the ratio of the nearby continuum to the scattering line intensity gives the albedo of the aluminum at that frequency. In theory, this can provide a direct, model independent albedo measurement technique. In practice, one must find a very optically thick line for which collisional quenching is very small and then correct for the

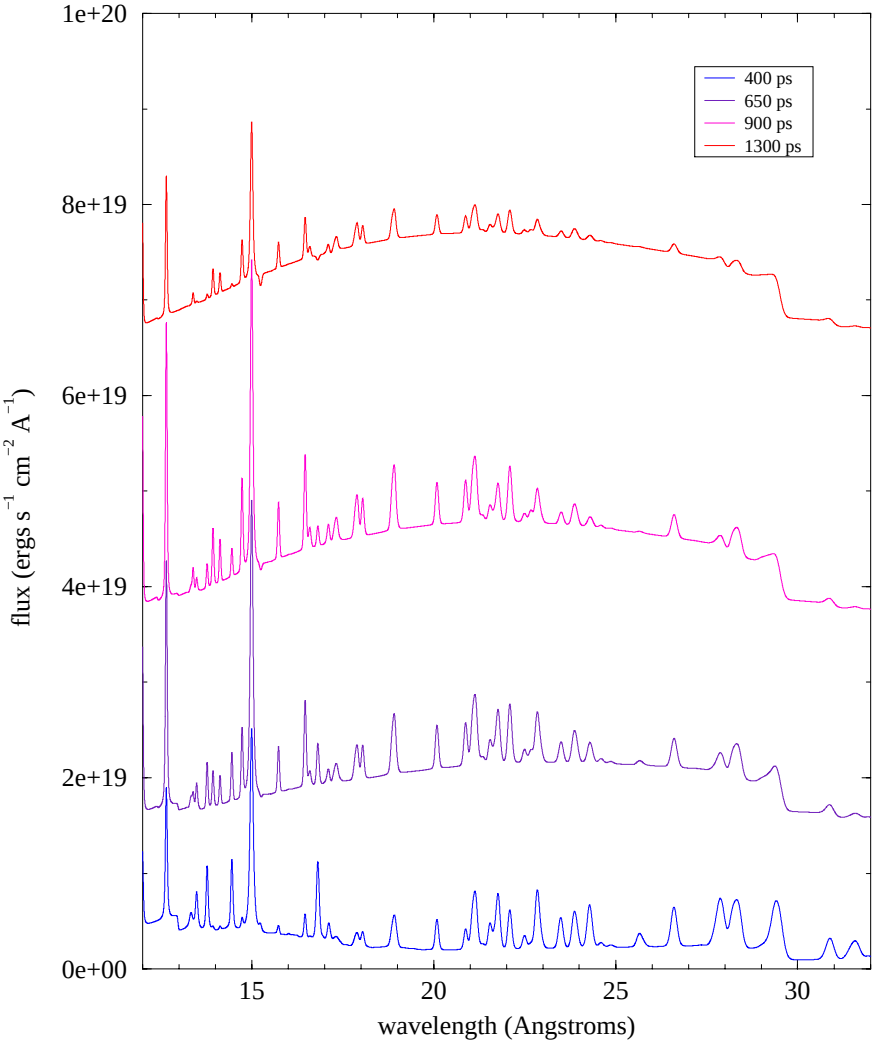

Figure 4.2. A time series of calculated spectra for shot 1504. These times correspond with the line-outs seen in the data plot. These models have been convolved with a Gaussian instrumental response having a FWHM of 3 eV, and are offset for clarity.

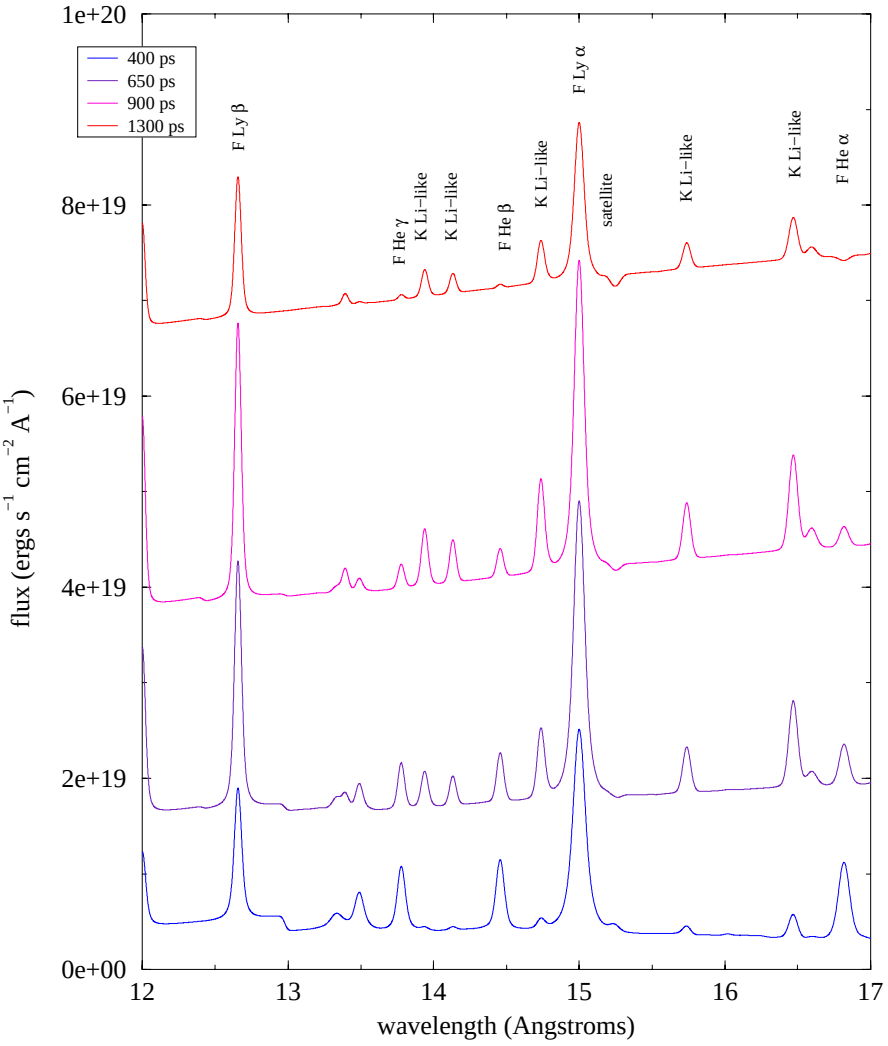

Figure 4.3. Expanded view of the models shown in the previous figure.

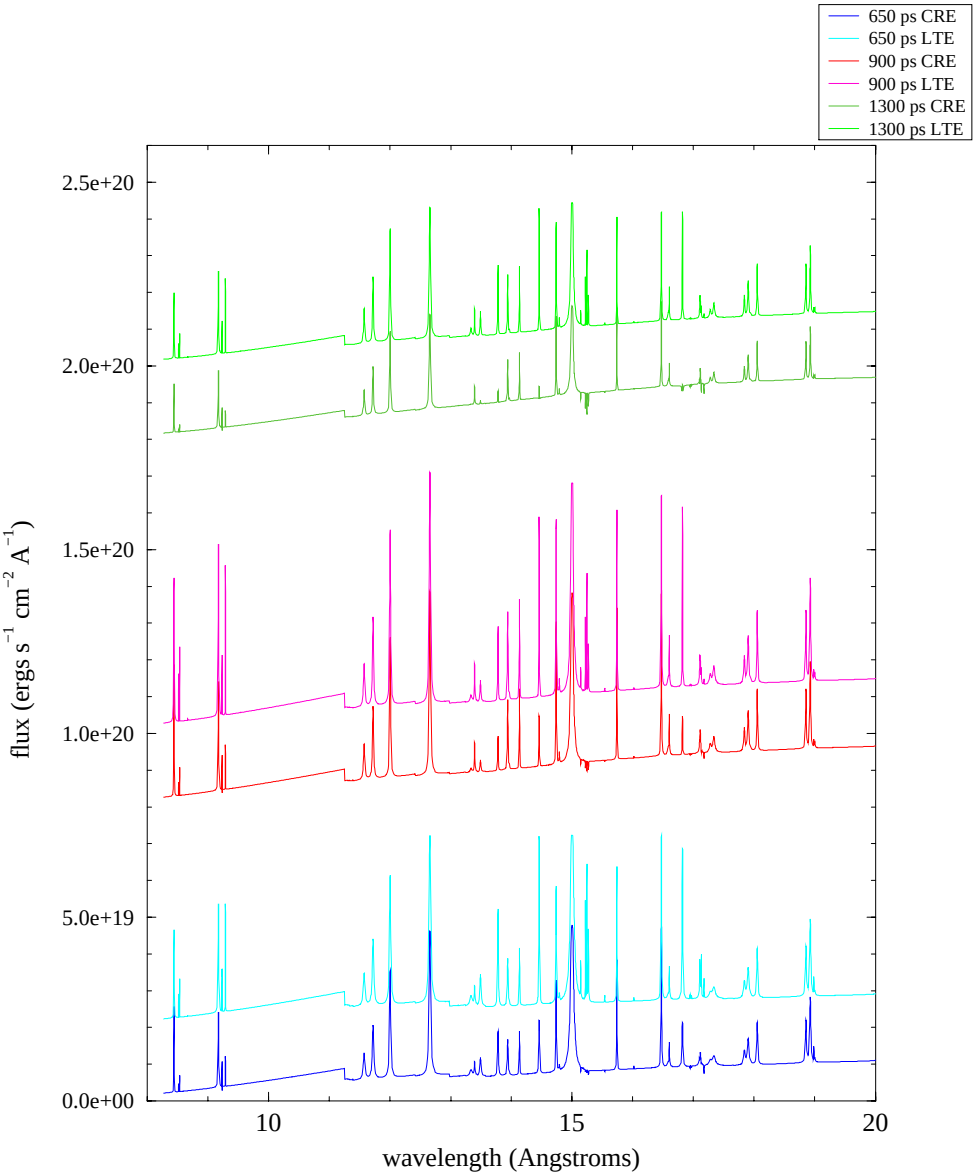

Figure 4.4. A comparison of LTE (top in each pair) and CRE (bottom in each pair) models of shot 1504 at the three later times shown in Figures 4.2 and 4.3.

effects of instrumental smearing. The effect of instrumental broadening on the F Ly$_\alpha$ line is shown in Figure 4.5.

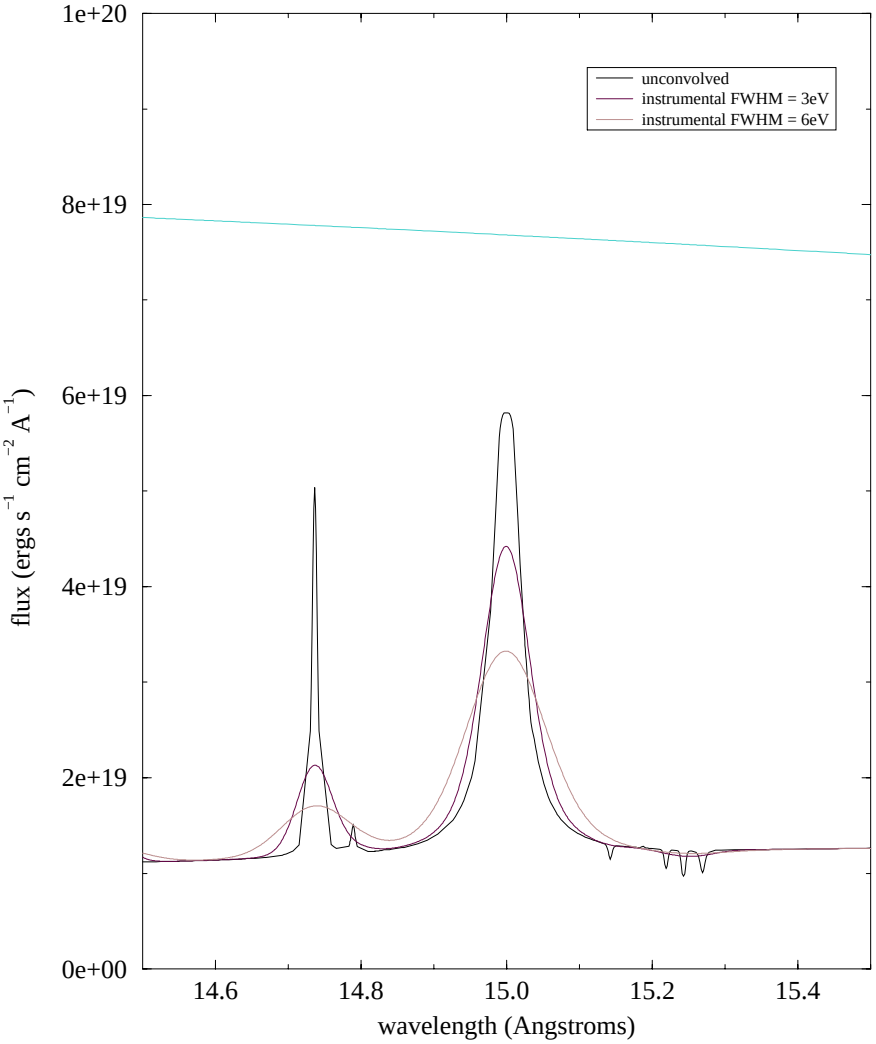

Figure 4.5. The F Ly$_\alpha$ line (at 15.0 Å) from a non-LTE calculation is shown with its natural line-width and also convolved with two different instrumental profiles. The blue line is the hohlraum (blackbody) radiation field.

5. Conclusions

The experiments performed in 1997 on the NOVA laser have shown that it is possible to spectrally observe line emission from buried tracers in hohlraums in the soft x-ray regime. The spectral properties evolve noticeably in time, and show the presence of gradients and non-LTE effects. Preliminary indications are that several different types of spectral diagnostics will be useful for diagnosing hohlraum radiation conditions and material properties of the witness plate.

Fluorine tracers provide a good spectroscopic signal in the sub-kilovolt range, with many strong K-shell lines. Potassium and chlorine L-shell emission is weaker, and the upper level populations may lag the radiation field. Tracer signals are easily seen even when the tracers are tamped under several microns of aluminum. A signal from the KCl layer was observed in at least one shot in which it was more than 11 μm from the hohlraum facing side of the witness plate. Signal from all the tracers is seen during the low-temperature ($T \approx 100$ eV) foot of the pulse shape 26 as well as during the peak of the shaped pulse and the square pulse ($T \approx 200$ eV) shots.

Our radiation-hydrodynamics modeling showed that the albedo-corrected DANTE data was consistent with the SOP shock breakout data to within the instrumental errors. This reconstructed radiation field can then be used as an input for the radiation-hydrodynamics and, ultimately, CRE modeling of the witness plates.

Albedo measurements using a scattering line, while theoretically possible, will require resolutions in excess of $\lambda/\Delta\lambda = 500$ if they are to truly be model independent. Satellite to resonance line ratios of F Ly_α features are density sensitive. The $2p - 4d$ lines of Li-like Cl and K are both visible in the spectral data and should be robust temperature diagnostics.

Spectral diagnostics from thin tracers buried in witness plates looks like a promising technique for understanding hohlraum and capsule physics. Future tracer spectral absorption experiments on the OMEGA laser should extend the range and power of these techniques.

Acknowledgments

This work was supported by the Department of Energy, NLUF program, under contract DE-FG03-96SF21015. We also received invaluable support from the NOVA technicians and scientists at LLNL.